RSC Advances

PAPER

View Article Online
View Journal | View Issue

Cite this: *RSC Adv.*, 2023, **13**, 674

Phosphomolybdic acid hydrate encapsulated in MIL-53 (Fe): a novel heterogeneous heteropoly acid catalyst for ultrasound-assisted regioselective nitration of phenols†

Ahmad Nikseresht,*[a] Rasoul Bagherinia,[a] Masoud Mohammadi[b] and Reza Mehravar[a]

In this study, a heterogeneous catalyst, PMA@MIL-53 (Fe) (MIL ⇒ Matériaux de l'Institut Lavoisier), has been used to replace the usual mineral acids such as sulfuric acid. A wide variety of nitration methods require the use of a mixture of acids such as concentrated nitric acid and sulfuric acid, which result in producing a large amount of acidic waste. During recent years, the use of the heterogeneous system for the nitration of aromatic compounds has been highly considered and used by chemists due to some specific advantages, *i.e.* easy separation of the product from the reaction mixture, the possibility of recycling and reusing the catalyst, *etc.* Herein, the catalyst was synthesized using a metal–organic framework and a heteropoly phosphomolybdic acid. The PMA@MIL-53 (Fe) was prepared using a similar method of MIL-53 (Fe) synthesis. Afterwards, $FeCl_3 \cdot 6H_2O$ and 1,4-benzene dicarboxylic acid (BDC) in a dimethylformamide solution were placed in an ultrasound bath and, then, HPA (heteropoly acid) was added to the reaction mixture. The PMA (phosphomolybdic acid) encapsulation in MIL-53 (Fe) was confirmed using various analysis. Under optimal conditions, the catalytic activity of PMA@MIL-53 (Fe) was evaluated in nitration of phenol under ultrasonic waves. Besides, the ratio of the two products of *ortho* and *para* was obtained using GC. Optimum conditions were reached after 15 minutes, in such a way that the loaded PMA was 0.02 g under optimal conditions, the efficiencies of *ortho*-nitrophenol and *para* nitrophenol were 54.98 and 45.01, respectively.

Received 7th November 2022
Accepted 5th December 2022

DOI: 10.1039/d2ra07077d

rsc.li/rsc-advances

1. Introduction

The aromatic nitration reactions can be considered as one of the most industrially important organic reactions due to adding a nitrogen substituent to the aromatic rings without the double-nitration by-products under mild reaction conditions.[1–3] In this sense, only a single nitro substitution has been added to the aromatic ring unless there is also a strong activating substituent.[4,5]

Nitrated phenols are one of the most important classes of the substituted aromatic compounds.[6] Besides, they are important synthetic intermediates and essential starting materials in advanced organic material synthesis, *i.e.* their reduction was a useful route to the corresponding amino-phenols and synthesis of phenol-containing natural products.[7,8] Although there are several multistep total synthesis and catalytic methods to achieve nitrophenol compounds, the one-pot reaction between a very powerful nitration reagent (*i.e.* conc. HNO_3 & H_2SO_4, N_2O_5 or NO_2/O_3 and metal nitrates) and phenol derivatives, in the presence of a solid acid as catalyst, is to a great extent accomplished as an intensively explored industrial method.[4,9–13] The mechanistic studies show that these reactions proceed through a nitronium ion (NO_2^+) which is attacked by π electrons delocalized around the aromatic rings leading to breakage of one of the N=O bonds to avoid a five-valent nitrogen.[14–16] Although the nitration of phenol is also very fast, these methods are not selective for the direct nitration of phenol, producing a mixture of *ortho*- and *para*-nitrophenols.[1] Besides, dilute nitric acid must be used to avoid the oxidation and over-oxidation of phenols to unspecified resinous products. Furthermore, because of the presence of strong activating OH groups on the starting arenes, overnitration (double nitration) to di-nitro aromatics is possible.[17–19]

To address the above issues and to enable a practical nitration process, researchers have been trying to optimize the

[a]*Department of Chemistry, Payame Noor University (PNU), 19395-4697 Tehran, Iran. E-mail: ahmad.nikseresht@pnu.ac.ir; a_nik55@yahoo.com*

[b]*Department of Chemistry, Faculty of Science, Ilam University, P. O. Box 69315516, Ilam, Iran*

† Electronic supplementary information (ESI) available. See DOI: https://doi.org/10.1039/d2ra07077d

selectivity and efficiency of this reaction using catalytic methods.[20–22] But, they need equivalents of strong acid-catalysis, operated at very high temperatures.[12,23–26] Considerably, drastic reaction conditions would greatly limit the energy efficiency.[7] In addition, the reaction progress requires very powerful reagents, leading to the formation of by-products and limiting the reaction yield and selectivity.[27–29] Thus, the development of catalytic reactions under mild conditions using the ultrasound-assisted method as an ideal medium has attracted significant attention in the arena of nitration reactions, because the reactions can be carried out at room temperature, leading to a reduction in the by-products formation and increasing the efficiency of the main products.[30–36]

During recent years, metal–organic frameworks (MOFs) have been regarded as one of the most popular and useful catalysts for laboratory and commercial scale organic synthesis.[37–47] On the ecological side, MOFs have been known as the low-cost and green solid supports, applied to immobilize the soluble catalysts due to their crucial role in lowering the toxicity, having heterogeneous[48,49] high specific surface area, possessing porous nature and also structural diversity, being economically viable and also having safe and recyclable characteristics to synthesize organic molecules – leading to the synthesis of a wide variety of MOF catalysts,[50,51] *i.e.* MIL-53 (Fe) which is an Fe-based MOF with high thermal stability and a very high surface area. In this sense it has greatly attracted researchers because of its exceptional tunability and functionality.[52–57] Moreover, researchers have also aimed at designing effective functionalized MOF catalysts with organic and organometallic moieties.[48,57–62] These methods which were applied to modify various types of catalysts,[61] heteropoly acids and other transition metal-catalysts have been successfully encapsulated into the pores of MIL-53 (Fe). In addition, these composites signify the application of MOF-functionalized catalytic species in organic synthesis and functional group transformations.[63] Thus, catalytic complex connection to the metal–organic frameworks (MOFs) as support is a new strategy to modify physiochemical properties, pore size, surface area and topology of the target porous material moieties.[64–68]

During recent decades, heteropoly acid catalysts, regarded as a member of Keggin structure crystals, have attracted great attention in catalysis science owing to a variety of important advantages.[69–72] Therefore, researchers have focused on the synthesis of heterogenized heteropoly acids.[73–75] Accordingly, we would introduce a novel phosphomolybdic acid hydrate (PMA) encapsulated @MIL-53 (Fe) MOF using the co-synthesis method as a novel functionalized MOF catalyst.

Considering our interest in the synthesis and application of MOF-based heterogeneous catalysts – using natural raw materials; herein, we aim at proposing the synthesis of PMA@MIL-53 (Fe) and its application in the direct nitration of phenol to the related nitro phenol derivatives in high yield and selectivity under ultrasonic waves.

2. Experimental section

2.1. Chemicals

Thin layer chromatography (TLC with silica gel plates 60F-254) was used to identify the desired compounds, improve the reactions, determine the reaction time and ensure the purity of the products and initial materials.

Solvents and other reagents were of analytical grade and utilized without further purification. In this study, all of the materials, reagents and solvents were obtained from Merck, Fluca, and Sigma Aldrich.

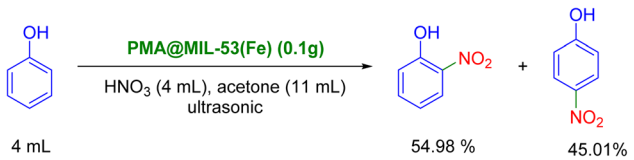

Scheme 2 Nitration of phenol by PMA@MIL-53 (Fe) catalyst.

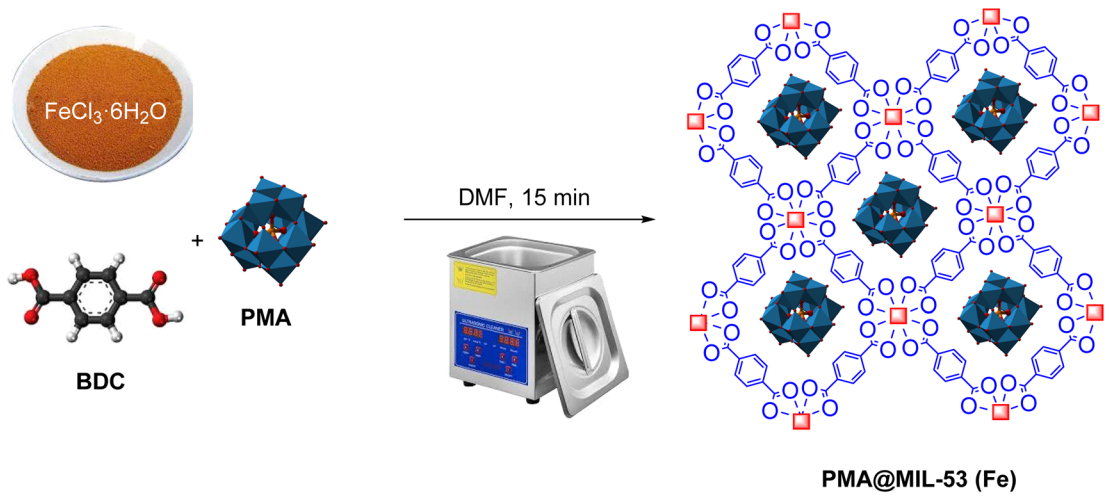

Scheme 1 Synthesis of PMA@MIL-53 (Fe) catalyst.

2.2. Instrumentation

GC model 7890B Agilent was equipped with column Rtx@5MS (length 30 m, internal diameter 0.25 mm). X-Ray powder diffraction spectrometer (diffraction type: D8 advance broker, $\lambda = 1.5406$ Å) was used to identify the solid sample. Thermal analysis of the samples was performed with Netzsch-TGA 209 F1. Fourier transformed infrared (FTIR) spectra were recorded using the FT-IR Spectrometer 470 Shimadzu using KBr pellets. The vibrational frequencies in the unit are wavelengths (cm^{-1}). XPS spectra were recorded on a Bes Tek spectrometer with A1 Kα X-rays as photon source (1486.6 eV). N_2 adsorption–desorption isotherm was used to determine the specific surface areas in Brunauer–Emmett–Teller (BET) at liquid nitrogen temperature (Micromeritics ASAP 2000). The weight percentage of hetero poly acid which was loaded in the pores and cavities was measured using a pair of induced plasma spectroscopy (ICP) and the Optima 8000 ICP-OES. The surface morphology of the composite was investigated applying scanning electron microscopy (SEM), (LEO 1430VP models) and high resolution transmission electron microscopy (HR-TEM) (Zeiss Libra 120 models), ultrasonic waves were generated using a Sonic 6mx ultrasonic bath with a pulse power of 37 kHz.

2.3. Synthesis of metal–organic framework MIL-53 (Fe)

The synthesis of the metal–organic framework MIL-53 (Fe) using ultrasonic waves has been reported by Gordon *et al.*[76] First, 1.27 g (1 mmol) of $FeCl_3 \cdot 6H_2O$ and 1.166 g (1 mmol) of 1,4-benzenedicarboxylate (BDC) were dissolved with 5 mL of DMF in a 51 mL flask. Afterwards, the container was irradiated in ultrasonic bath for 15 minutes. The resulting powder was separated from the solution using centrifuge and, then, heated to 150 °C for 24 hours.

2.4. Synthesis of PMA@MIL-53 (Fe) using ultrasonic waves

PMA@MIL-53 (Fe) is synthesized using a method similar to MIL-53 (Fe) synthesis. In this sense, heteropoly acid was added to the reaction medium. Moreover, capsulation was occurred in MIL using interaction of facial cavity walls. Primarily, 1.27 g (1 mmol) of $FeCl_3 \cdot 6H_2O$ and 1.166 g (1 mmol) of 1–4 benzene decarboxylic acid (BDC) with 5 mL of DMF were completely

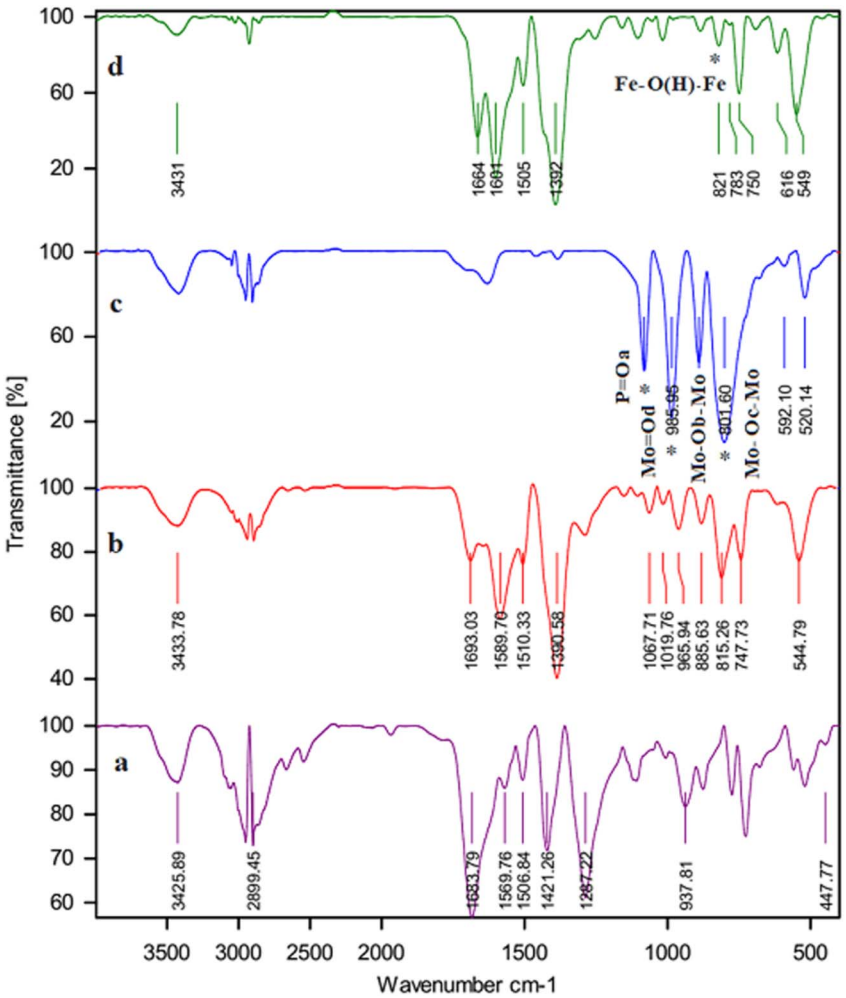

Fig. 1 FT-IR spectrum (a) H2BDC, (b) MIL-53 (Fe), (c) PMA and (d) PMA@MIL-53 (Fe).

dissolved in several flasks. Subsequently, different amounts of phosphomolybdic acid hydrate (PMA) (0.01 and 0.02 g) were added to each container and, then, placed in the ambient temperature for 15 minutes under ultrasonic radiation. At the end of the reaction, the synthesized compound was separated using centrifuge and, then, heated for 15 hours at 150 °C (Scheme 1).

2.5. Nitration of phenol by PMA@MIL-53 (Fe) catalyst

The catalytic activity of PMA@MIL-53 (Fe) was investigated using the phenolic nitration reaction under ultrasonic waves. In this sense, 11 mL acetone, 4 mL phenol, 4 mL nitric acid and 0.1 g of catalyst were added to the flask (25 mL). The reaction was performed in an ultrasonic bath under ultrasonic irradiation. It is worth mentioning that ultrasonic waves provide the energy for the reaction and the temperature was fixed at room temperature by pouring cold water in the bath. The progression of the reaction was investigated using TLC. Moreover, the catalyst was separated using centrifuge after the end of the reaction. The efficiency of the reaction and the percentage of isomers *ortho* and *para* were determined using GC as reported in ESI† (Scheme 2).

3. Results and discussion

3.1. Characterization of catalyst

In order to confirm the encapsulation of the PMA compound in MIL-53 (Fe), the FT-IR, XRD, XPS, TGA, EDS, ICP-OES, X-ray mapping, Fe-SEM, HR-TEM and nitrogen adsorption–desorption characterization techniques were used.

3.1.1. The results of FT-IR. FT-IR spectroscopy confirmed the addition of PMA to the framework structure, as shown in Fig. 1. The comparison of the two FT-IR spectra of the bed and the PMA@MIL-53 (Fe) show that the appearance of new peaks at 792, 889, 968, and 1063 cm^{-1} correspond to the PMA@MIL-53 (Fe). The peaks at 789 888, 969 and 1059 cm^{-1} are attributed to the vibrations of –P–O, Mo–Oe–Mo and Mo–Oc–Mo. Comparison of the spectra shows that heteropoly acid is well located in the composite structure. Moreover, the vibrational frequency has a slight change due to the interactions of heteropoly acid with the framework. Thus, it can be concluded that the capsule process is well performed.

3.1.2. X-Ray diffraction (XRD). Powder XRD measurements were performed using a diffraction spectrometer (diffraction type: D8 advance broker, $\lambda = 1.5406$ Å). Fig. 2 shows that the XRD pattern for PMA, MIL-53 and PMA@MIL-53 are similar to previous reports. There are minor changes in the XRD pattern as compared to MIL-53 (Fe) due to capsulation heteropoly acid. These changes show that PMA is encapsulated in the framework. XRD patterns indicate that MIL-53 structure is not destroyed and structural characteristics are preserved during the process of encapsulating.

3.1.3. X-Ray photoelectron spectroscopy (XPS) analysis. XPS analysis was performed to study the elemental composition and chemical states of PMA@MIL-53 (Fe) MOF (Fig. 3). The XPS survey spectra show the presence of Fe, C, and O elements in the prepared sample that is in good agreement with the previous report on its patent MOF (MIL-53 (Fe)). The high-resolution XPS spectra show two peaks at around 713.1 eV and 726.3 eV binding energy which are attributed to the Fe 2p (Fe $2p_{3/2}$ and Fe $2p_{1/2}$ of Fe(III)), respectively. The comparison of the XPS spectra of the PMA@MIL-53 (Fe) MOF to its parent MIL-53 (Fe) shows a slight shift on Fe peaks along with the appearance of new peaks at 233.4 eV and 235.8 eV corresponding to the Mo due to the interactions of heteropoly acid with the framework. This result confirms the addition of PMA to the MIL-53 (Fe) MOF.

3.1.4. The results of thermal gravimetric analysis (TGA). Thermal behavior of H_2BDC, MIL-53 (Fe) and PMA@MIL-53 was investigated using TGA analysis. Besides, the obtained data are presented in Fig. 4. Regarding the curves, two major weight losses were observed. The first stage is at temperature below 211 °C which can be due to the removal of some moisture in the samples and DMF in the MOFs cavities. In addition, the H_2BDC is stable at up to 285 °C and, significantly, it was completely decomposed from 300 to 375 °C. In this sense, it is worth mentioning that it was selected as our reference for the decomposition of organic groups in the prepared samples. Regarding the TGA curves of MIL-53 and PMA@MIL-53 comparison, it is clear that the weight loss of PMA@MIL-53 is much less than that of H_2BDC and MIL-53 (Fe) respectively, which is due to the heteropoly acid place in the cavities of the framework. It is well concluded that the encapsulation process

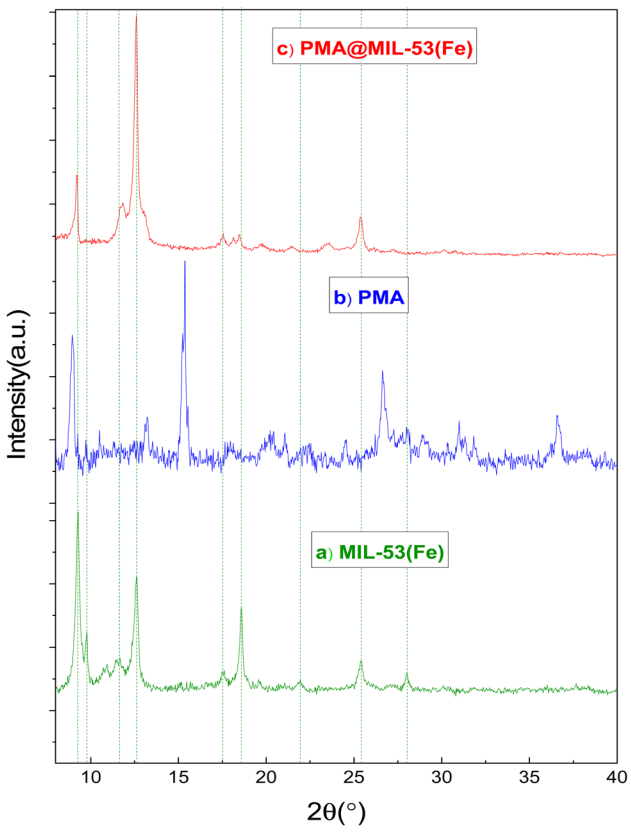

Fig. 2 XRD patterns (a) MIL-53 (Fe) and (b) PMA (c) PMA@MIL-53 (Fe).

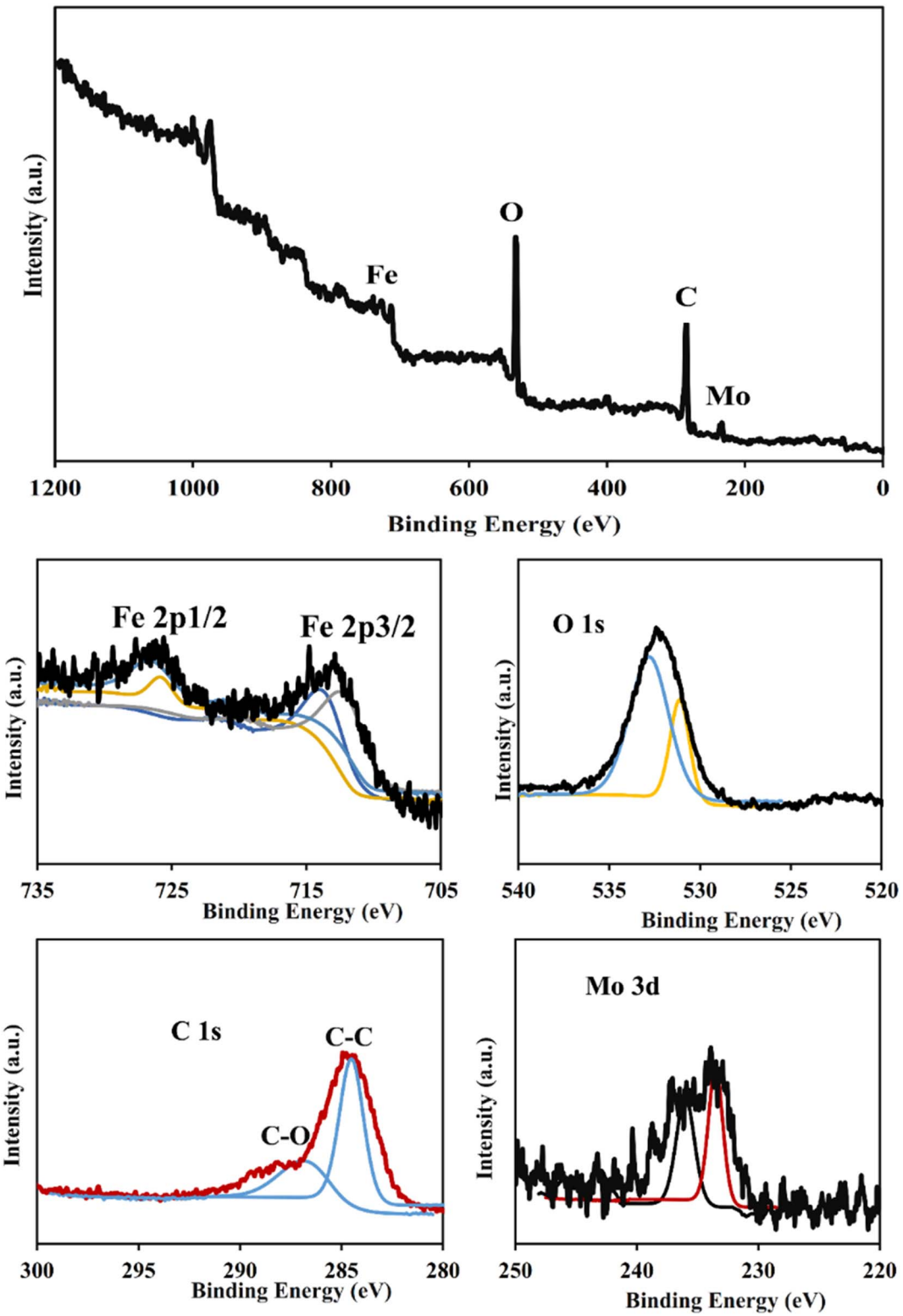

Fig. 3 XPS analysis of PMA@MIL-53 (Fe).

of PMA heteropoly acid has been successfully performed. In addition, the thermal stability of the sample increased *via* PMA addition to the structure.

3.1.5. Energy-dispersive X-ray spectroscopy. The elemental composition of the synthesized MIL-53 (Fe) (b) PMA@MIL-53 (Fe) composites was carried out using EDX analysis (Fig. 5). The EDX measurements indicate that all of the required

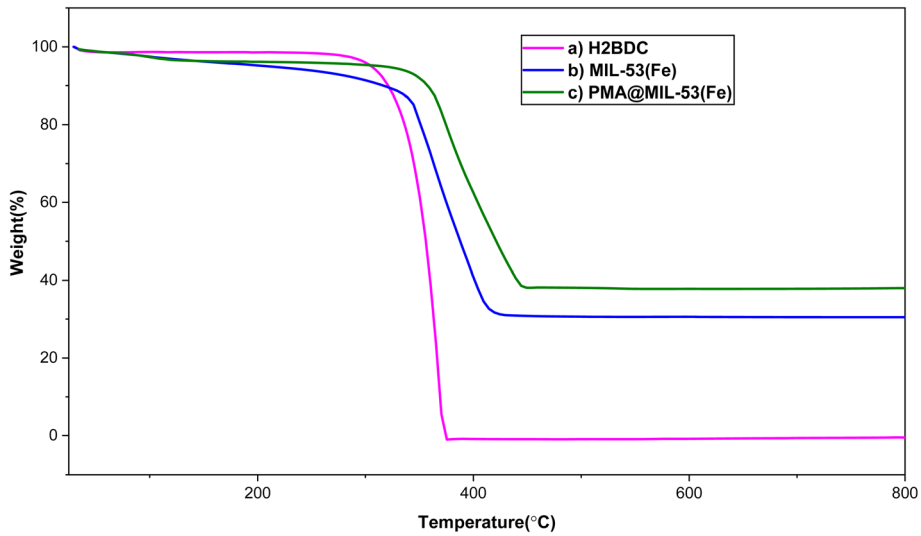

Fig. 4 TGA curves of (a) H_2BDC, (b) MIL-53 (Fe) and (c) PMA@MIL-53.

elements, including C ($k\alpha = 0.277$ keV), O ($k\alpha = 0.525$ keV) and Fe ($L\alpha = 0.705$, $k\alpha = 6.924$ and $k\beta = 7.07$ keV) species in MIL-53 (Fe), confirm the formation of the targeted MOF material. Additionally, the EDX measurements on PMA@MIL-53 (Fe) composites represent that, all of the X-ray signals of its parent MOF material, the position of a sharp peaks of Mo ($L\alpha = 2.293$ keV) and P ($K\alpha = 2.013$ keV) elements is attributed to PMA segments. These results confirm the encapsulation of PMA nanostructures into MIL-53 (Fe) metal–organic frameworks and the successful formation of the target heteropoly acid heterogeneous catalyst.

3.1.6. Inductively coupled plasma mass spectrometry. Inductively coupled plasma analysis of PMA (10 wt%) @MIL-53 (Fe) indicates that the sample contains 60 985 ppm of molybdenum, while molybdenum forms 63.075 wt% of phosphomolybdic acid (PMA). Regarding that 1 wt% = 10 000 ppm, the amount of molybdenum is 6.0985 wt in this sense, the amount of molybdenum – as equivalent to phosphomolybdic acid – must be calculated. Therefore, by dividing 6.0985 (wt% Mo) by 63.075 and multiplying it by 100, the amount of PMA is obtained as 9.67 wt% (the actual value of the loaded PMA). It should be noted that there is often a difference between theoretical values and actual values of the loaded PMA in composite. As shown in Table 1, in higher values of PMA, the amount of this difference is greater. The reason for this difference is logical and predictable. Accordingly, two main reasons (in addition to minor systematic and individual errors) can be presented: (a) for many reasons that are beyond the scope of this discussion,

Table 1 The characteristics of PMA@MIL-53 (Fe) composite

Entry	Sample	Mo (ppm)	Actual loading of PMA (wt%)
1	MIL-53 (Fe)	—	—
2	PMA (10 wt%)@MIL-53 (Fe)	60 985	9.67
3	PMA (20 wt%)@MIL-53 (Fe)	121 545	19.27

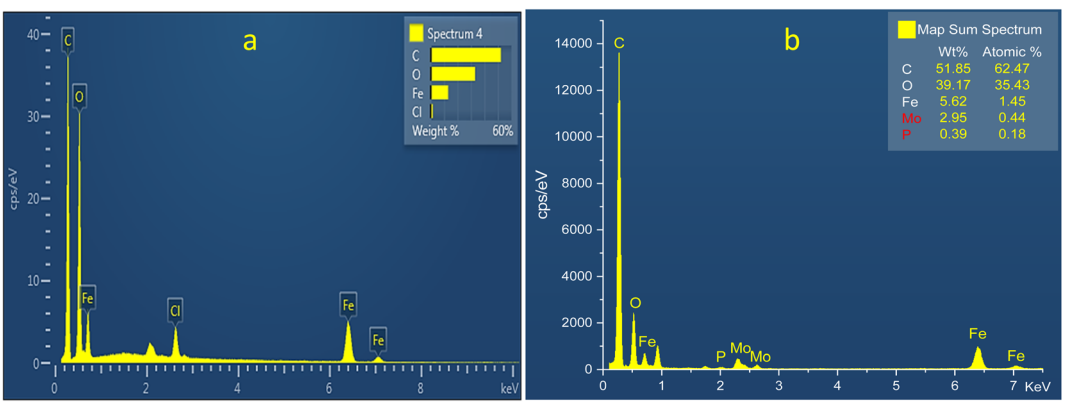

Fig. 5 EDS analysis of (a) MIL-53 (Fe) (b) PMA@MIL-53 (Fe).

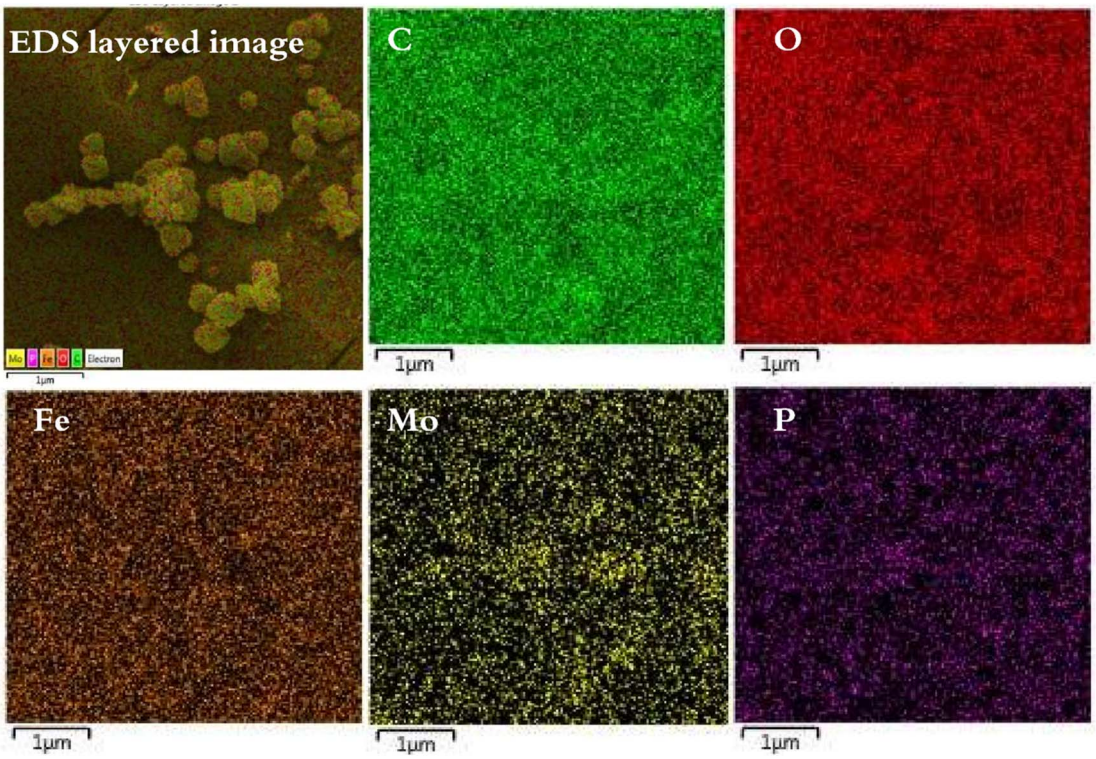

Fig. 6 X-Ray mapping analysis of PMA@MIL-53 (Fe).

the distribution of PMA in MIL-53 (Fe) cavities is random, and we cannot assume a uniform distribution for PMA in the MIL-53 (Fe) structure. For example, we cannot say that all holes of MIL-53 (Fe) are filled by PMA. (b) The second major reason is related to the sampling of the synthesized composite. Therefore, the difference of the samples in the analysis causes more influence of the factor, the non-uniformity of PMA distribution in MIL-53 (Fe) and as a result, it will be an influential factor in the observed error.[77]

3.1.7. Elemental mapping analysis. In addition, the distribution of the elements was investigated using EDX-mapping analysis (Fig. 6). Elemental mapping images revealed the high density of C, O and Fe elements as the MOF support and also the high content of Mo and P elements as being uniformly distributed around the composite system, confirming the formation and excellent accessibility of the encapsulated heteropoly acid catalyst.

3.1.8. Scanning electron microscopy (SEM). The morphology of the catalyst was observed using scanning electron microscopy (SEM) (LEO 1430VP models). Fig. 7 shows the structure of MIL-53 (Fe) before and after the capsulation PMA. The results show that with the addition of hetero poly acid to the framework, the surface became rough and uneven, which indicates the presence of PMA. Based on the results, it is assured that the hetero poly acid was located in the pores of the framework.

3.1.9. High resolution transmission electron microscopy (HR-TEM). The particle size and morphology of the PMA@MIL-53 (Fe) composite were measured using HR-TEM analysis (Fig. 8). The obtained high magnification TEM graphs illustrated that the size distribution of the MIL-53 (Fe) crystals is not uniform and crystal sizes ranged from 200–500 nm. The magnified TEM image reveals that very small black particles in different sizes (1–2 nm) were closely attached to the surface of the MIL-53 (Fe) crystals, which indicate the existence of PMA in the PMA@MIL-53 (Fe) composite. The above results show that the MIL-53 (Fe) was well prepared and PMA functionalities have successfully encapsulated onto its pores.

3.1.10. Nitrogen adsorption–desorption measurements. The porosity properties of the prepared PMA@MIL-53 (Fe) composite were measured using nitrogen adsorption–desorption analysis (Table 2). Surface areas, pores volumes and average pore sizes of the catalysts were measured using N_2 physi-sorption and Micromeritics ASAP 2000. Fig. 5 shows the nitrogen adsorption–desorption isotherms of the PMA@MIL-53 (Fe) framework. The results show that, with the addition of PMA, the total pore volume (V_{total}) and mean pore diameter (D_{mean}) decreased from 0.067928 $cm^3\ g^{-1}$ to 0.0215 $cm^3\ g^{-1}$ and 18.23 to 16.784 nm, respectively. It is worth to mention that according to literature,[78] MIL-53 (Fe) only opens its pores in the presence of guest molecules; therefore, unlike MIL-101 it does not have a high surface area. Additionally, in this work the surface area of pure MIL-53 (Fe) is significantly bigger than that of earlier reports on identical samples that were produced under optimal conditions.[79] It can also be seen from Table 2 that the surface area decreases from 320 ($m^2\ g^{-1}$) to 136.39 (m^2

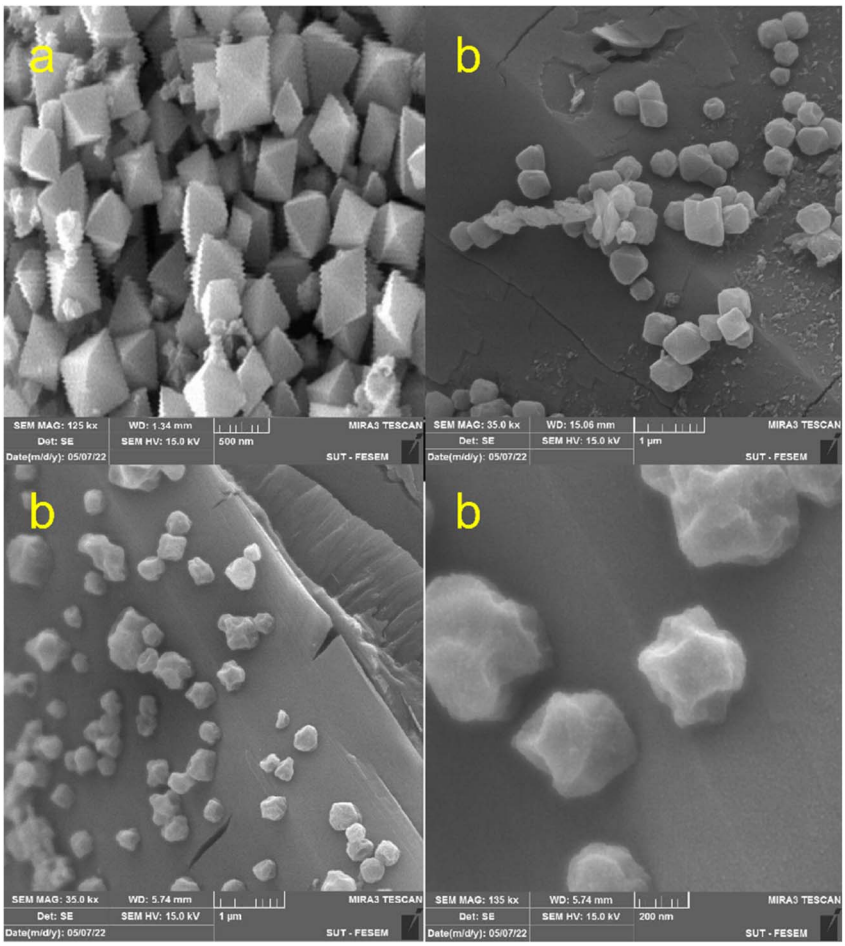

Fig. 7 SEM image of (a) MIL-53 (Fe) and (b) PMA@MIL-53 (Fe).

g^{-1}) for MIL-53 (Fe) and PMA (20 wt%)@MIL-53 (Fe), due to the presence of heavy phosphomolybdic moieties.[80] This evidence confirms the encapsulation of PMA and the formation of the composite (Fig. 9).

3.2. Catalytic study

3.2.1. Optimization the nitration of phenol. Regarding the significance of nitrated phenol derivatives, the possibility of phenol nitration was investigated using the high scale electrophilic aromatic substitution reactions of phenol with nitric acid. Besides, we also applied PMA@MIL-53 (Fe) MOF as an effective heterogeneous heteropoly acid catalyst. In this sense, the effect of various reaction parameters (*i.e.* catalyst loadings and reaction time) was investigated. Accordingly, the results are shown in Table 3.

The present study was initiated using the reaction of phenol (4 mmol) with nitric acid (4 mmol) as the model reaction in 10 mL of acetone as solvent and in presence of 0.1 g of PMA@MIL-53 (Fe) catalyst (Table 1) under ultrasonic irradiation for different reaction times. The transformation process with the reaction time for the nitration reaction was monitored using TLC and, then, the yields were calculated using gas chromatography (GC). It was observed that, while increasing the required reaction time, product yield was also increased. These results show that time plays a critical role in this catalytic reaction. In addition, a clear difference was found in the reaction selectivity and efficiency under different reaction times (entries 1–3, Table 3). Moreover, 95.62% yield of the *ortho*- and *para*-mononitrophenols mixture was concurrently obtained in 15 min (*ortho*/*para* ratio was 54 : 46). Afterwards, the effect of PMA loading on the reaction was evaluated (Table 3 entries 4–6). It was observed that when the concentration of PMA in the catalyst increased to 20 mg the time required for the completion of the reaction decreased. It was found out that the increase in PMA loading in MOF catalyst improves the reaction yield (up to 99.99%) and selectivity (*ortho*/*para* ratio was 55 : 45) which suggests that the phenol substrate is almost completely converted to its corresponding mononitrated *ortho*- and *para*-nitrophenols. These results show that the PMA plays a critical role in this catalytic reaction. Hence, the results also show that *ortho*/*para*-nitrophenols can be effectively prepared in presence of PMA@MIL-53 (Fe) (including 20 mg of PMA content) catalyst in acetone solvent system at room temperature, giving good

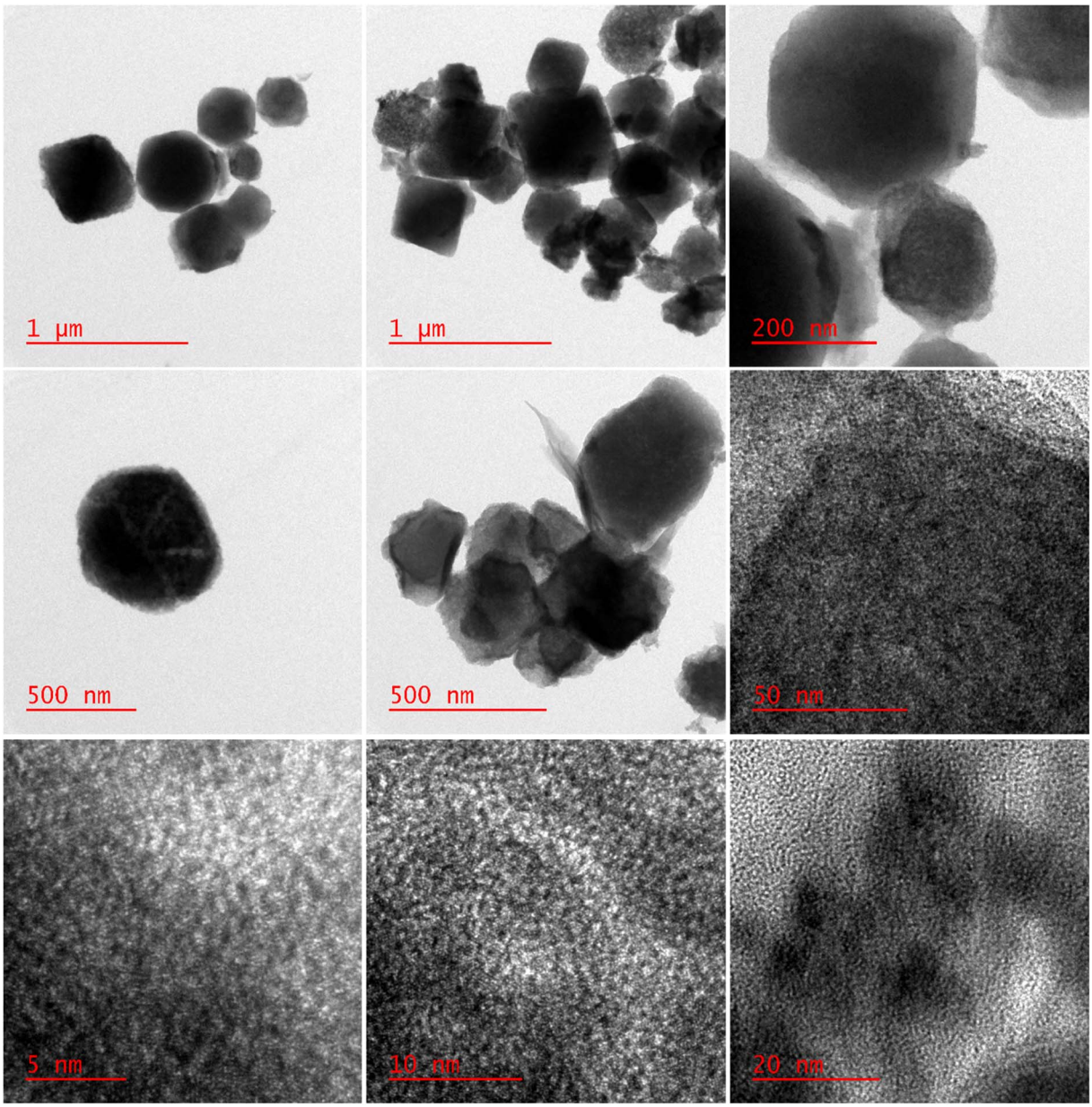

Fig. 8 HR-TEM images PMA@MIL-53 (Fe).

Table 2 Summarized characteristics of PMA@MIL-53 (Fe) composite and its parents

Entry	Sample	S_{BET}[a] (m^2 g^{-1})
1	MIL-53 (Fe)	320
2	PMA (10 wt%)@MIL-53 (Fe)	218.2
3	PMA (20 wt%)@MIL-53 (Fe)	136.39

[a] Specific surface area.

yield in less reaction time (Table 3). Finally, the results of these catalytic investigations indicated that the *ortho*-nitro product was formed easier than its *para*-nitro isomer and provided the corresponding products in higher yields. Moreover, it is worth mentioning that the reaction involved a slight *ortho*-selectivity for all of the tested reactions. The exact explanation for this selectivity is due to the hydrogen bonding in its related intermediate, which causes stability and ease of formation. It is worth to mention that the reaction was evaluated in the absence of HNO_3 or the absence of catalyst, in both cases the reaction process stalled.

3.3. Mechanism

The plausible mechanism of the phenol nitration reaction in presence of the PMA@MIL-53 (Fe) acid-catalyst is shown in Scheme 3. It encompasses two-steps: first, generating nitronium ion (NO_2^+) *via* acid-catalyzed water elimination from nitric acid and, then, electrophilic substitution reaction. In the second

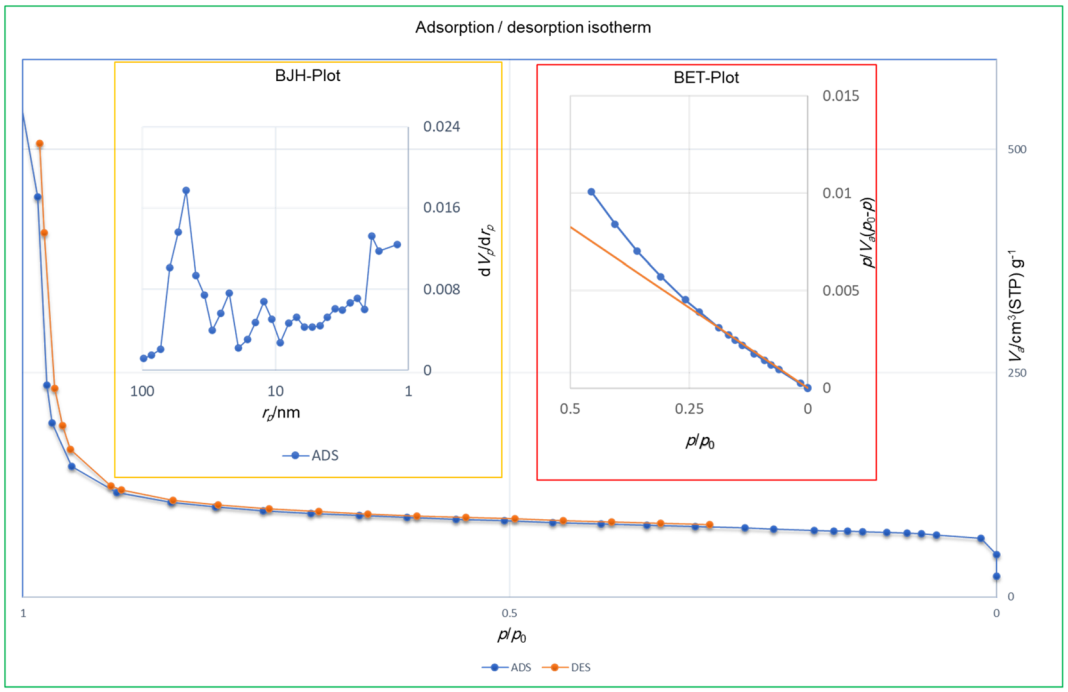

Fig. 9 Surface area, pore volume and pore size distribution curves of PMA@MIL-53 (Fe).

Table 3 Screening the reaction parameters for the nitration of phenol under the catalysis of PMA@MIL-53 (Fe)

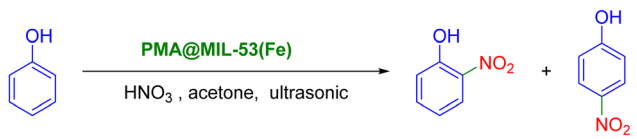

Entry	Catalyst	Time (min)	Yield[a,b,c] (%) Total	*Ortho*	*Para*
1	—	5	NR	—	—
2	MIL-53 (Fe)	5	NR	—	—
3	PMA (10 wt%)@MIL-53 (Fe)	5	29.5	16.41	13.09
4	PMA (10 wt%)@MIL-53 (Fe)	10	75.13	41.11	34.02
5	PMA (10 wt%)@MIL-53 (Fe)	15	95.62	51.91	43.71
6	PMA (20 wt%)@MIL-53 (Fe)	5	38.54	20.71	17.83
7	PMA (20 wt%)@MIL-53 (Fe)	10	76.94	44.02	32.92
8	PMA (20 wt%)@MIL-53 (Fe)	15	99.99	54.98	45.01
9	PMA (20 wt%)@MIL-53 (Fe)	15	NR[c]	—	—

[a] GC yields. [b] Conditions: phenol (4 mL), nitric acid (4 mL) PMA@MIL-53 (Fe) (100 mg) in acetone (10 mL) at room temperature under ultrasound irradiation. [c] The reaction in the absence of HNO_3.

step, the π electrons were delocalized around the aromatic rings, leading to break one of the N=O bonds to avoid a five-valent nitrogen, finally the removal of a proton from the substituted carbon leads to the aromatization of products.

3.4. Recovery and reusability

As an added benefit of PMA@MIL-53 (Fe), it can be recovered and reused for the same reaction several times. Herein, PMA@MIL-53 (Fe) was separated from the reaction mixture by centrifugation, rinsed multiple times with ethanol, dichloromethane and acetone, dried at 80 °C under vacuum and, further, reused straightforwardly for the fresh nitration reaction. Based on the result of its recyclable catalytic effectiveness, this became clear that the catalyst has such an excellent catalytic influence even after becoming reused for 8 attempts (Fig. 10). In addition, SEM and FT-IR spectra of the recovered catalyst were compared with the fresh one that showed no morphological, functionalities changes respectively (Fig. 11a and b), thus providing a strong evidence for excellent durability and stability of the catalyst.

3.5. Hot filtration test

The heterogeneous nature was investigated using a hot filtration study of the PMA@MIL-53 (Fe) catalyst under optimum operating conditions to determine whether PMA was leaching out or not from MIL-53 (Fe). This test reveals that the leaching of PMA did not take place after the reaction, clarifying that the PMA was still bound to the MIL-53 (Fe) framework. This provides strong evidence of its structural stability and gives good results even after its multiple reuses.

3.6. Comparison

We have also compared the efficiency of our catalyst with some literature reports. The catalyst is effective against the nitration reaction under milder conditions at shorter reaction time and

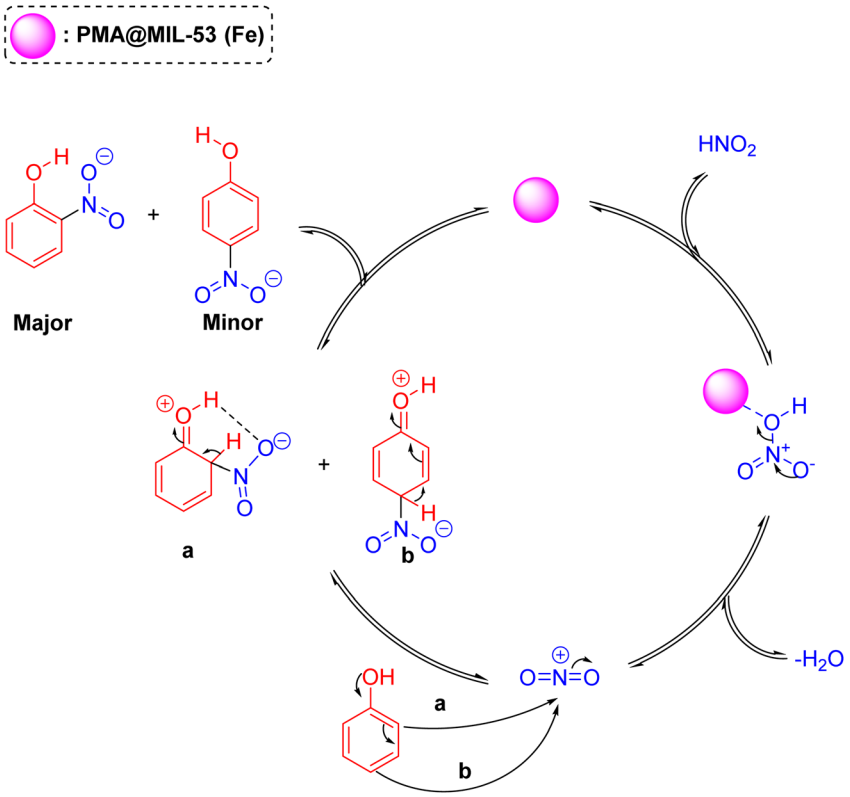

Scheme 3 Plausible mechanism for the nitration of phenol catalyzed by PMA@MIL-53 (Fe) solid acid.

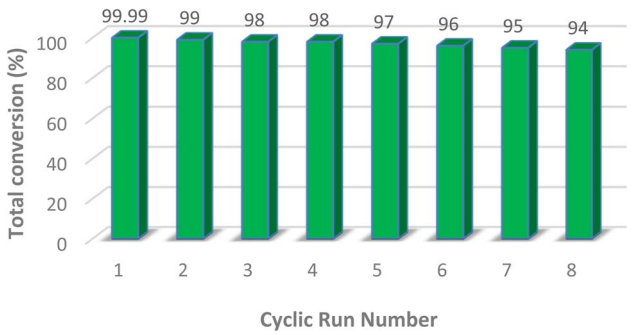

Fig. 10 Reusability of PMA@MIL-53 (Fe) catalyst.

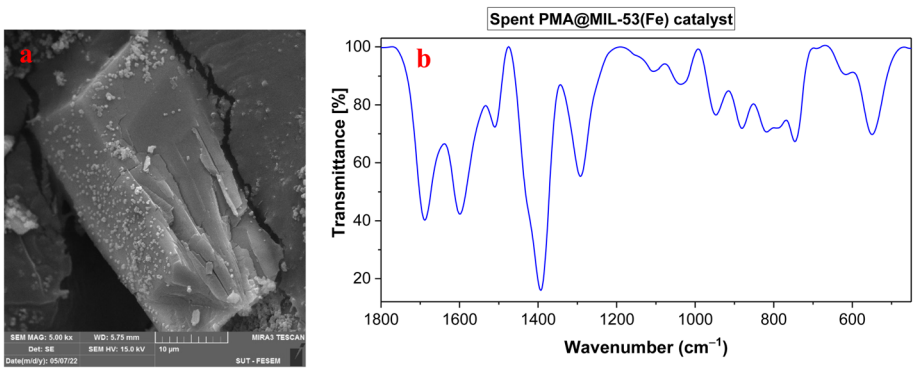

Fig. 11 (a) SEM image and (b) FT-IR spectrum of the recovered PMA@MIL-53 (Fe) catalyst.

Table 4 Comparison of the catalytic activity of PMA@MIL-53 (Fe) in the nitration of phenol with other reported catalyst systems in the literature

Entry	Catalyst	Time (min)	Yield (%)			Ref
			Total	*Ortho*	*Para*	
1	Montmorillonite KSF	60	84	44	40	81
2	Tetrabutylammonium chromate	2880	80	44	36	82
3	$[KHSO_4 \cdot 2KHSO_5 \cdot K_2SO_4]$	180	79	40	39	83
4	Cerium(IV) ammonium nitrate (CAN)	1440	69	28	41	84
5	Silica sulfuric acid	25	79	36	43	85
6	PMA@MIL-53 (Fe)	15	99.99	54.98	45.01	This work

higher yields with more regioselectivity and reusability (Table 4). It shows the uniqueness of the PMA@MIL-53 (Fe) heterogeneous catalyst over other catalysts.

4. Conclusion

We have developed a novel heteropoly acid encapsulated in MOF support and explored its efficiency as catalyst for phenol nitration reactions. The mentioned catalyst shows good to excellent yields in acetone at room temperature. Moreover, this catalyst can be effortlessly removed from the reaction mixture *via* simple filtration or centrifugation and reused eight times which shows its stability, recyclability and longevity.

Conflicts of interest

There are no conflicts to declare.

References

1 K. A. Juárez-Ornelas, J. O. C. Jiménez-Halla, T. Kato, C. R. Solorio-Alvarado and K. Maruoka, *Org. Lett.*, 2019, **21**, 1315–1319.
2 B. T. Ergan, M. Bayramoğlu and E. Şahin, *Journal of Microwave Power and Electromagnetic Energy*, 2017, **51**, 314–324.
3 E. Bolzacchini, M. Bruschi, G. Galliani, J. Hjorth, M. Orlandi and B. Rindone, in *ACS National Meeting Book of Abstracts*, 2007.
4 Y. H. Sriram, T. Fatima, K. C. Rajanna, M. S. Kumar and R. M. Raju, *Int. J. Chem. Kinet.*, 2017, **49**, 622–632.
5 E. Bolzacchini, J. Hjorth, S. Meinardi, M. Orlandi, B. Rindone and E. Rosenbohm, in *ACS National Meeting Book of Abstracts*, 2000, vol. 40, pp. 395–397.
6 S. Mondal, J. Singh, S. Singh, S. Vishwakarma, K. Mitra, A. Kumari, R. Singh, S. K. Sen Gupta and B. Ray, *New J. Chem.*, 2020, **44**, 10878–10884.
7 C. Zhang, J. Dong, M. Liu, W. Zhao and D. Fu, *J. Hazard. Mater.*, 2019, **373**, 547–557.
8 C.-C. Du, X.-F. Wang, S.-B. Zhou, D.-Z. Wang and D. Jia, *CrystEngComm*, 2017, **19**, 6758–6777.
9 C. A. Bunton, E. D. Hughes, G. J. Minkoff and R. I. Reed, *Nature*, 1946, **158**, 514–515.
10 N. G. Tran, H. Kalyvas, K. M. Skodje, T. Hayashi, P. Moënne-Loccoz, P. E. Callan, J. Shearer, L. J. Kirschenbaum and E. Kim, *J. Am. Chem. Soc.*, 2011, **133**, 1184–1187.
11 T. C. Bruice, M. J. Gregory and S. L. Walters, *J. Am. Chem. Soc.*, 1968, **90**, 1612–1619.
12 M. A. Mondal, D. Mandal and K. Mitra, *J. Chem. Sci.*, 2017, **129**, 39–43.
13 M. R. Patil, P. H. Mohite, S. Shisodia and R. S. Keri, *Lett. Org. Chem.*, 2015, **12**, 129–135.
14 L. C. Raiford, *J. Am. Chem. Soc.*, 1922, **44**, 158–165.
15 M. Suresh, K. C. Rajanna, Y. H. Sriram and Y. R. Rao, *SN Appl. Sci.*, 2019, **1**, 485.
16 C. M. R. Rocha, J. A. R. Rodrigues, P. J. S. Moran and R. Custodio, *J. Mol. Model.*, 2014, **20**, 2524.
17 X. Cheng, Q. Chen, Y. Li, G. Huang, Y. Liu, S. Lu, Y. Zheng, W. Qiu, K. Lu, X. Qiu, F. Bianchi, C. Yan, B. Yuan, M. Shao, Z. Wang, M. R. Canagaratna, T. Zhu, Y. Wu and L. Zeng, *Environ. Sci. Technol.*, 2021, **55**, 4410–4419.
18 C. Wu, Q. Bian, T. Ding, M. Tang, W. Zhang, Y. Xu, B. Liu, H. Xu, H.-B. Li and H. Fu, *ACS Catal.*, 2021, **11**, 9561–9568.
19 R. S. Glass, *J. Chem. Educ.*, 1983, **60**, A283.
20 W. Zhang, J. Zhang, S. Ren and Y. Liu, *J. Org. Chem.*, 2014, **79**, 11508–11516.
21 M. Mohammadi, M. Khodamorady, B. Tahmasbi, K. Bahrami and A. Ghorbani-Choghamarani, *J. Ind. Eng. Chem.*, 2021, **97**, 1–78.
22 M. Mohammadi and A. Ghorbani-Choghamarani, *Appl. Organomet. Chem.*, 2022, **36**, e6905.
23 B. B. Thummar, U. P. Tarpada and D. K. Raval, *J. Heterocycl. Chem.*, 2014, **51**, 1740–1746.
24 S. P. N. Sudhan, R. N. Ahmed, H. Kiyani and S. S. Mansoor, *J. Saudi Chem. Soc.*, 2018, **22**, 269–278.
25 Z. L. Shen, X. P. Xu and S. J. Ji, *J. Org. Chem.*, 2010, **75**, 1162–1167.
26 V. Kumar, S. Ghosh, A. K. Saini, S. M. Mobin and B. Mondal, *Dalton Trans.*, 2015, **44**, 19909–19917.
27 A. Kalita, R. C. Deka and B. Mondal, *Inorg. Chem.*, 2013, **52**, 10897–10903.
28 B. Baghernejad, M. M. Heravi, H. A. Oskooie and F. F. Bamoharram, *Bull. Chem. Soc. Ethiop.*, 2012, **26**, 145–152.
29 Z. Tunalı, K. Sagdic, F. Inci and B. Ö. Öztürk, *React. Chem. Eng.*, 2022, **7**, 1617–1625.

30 H. Yu, Q. Zhong, Y. Liu, Y. Guo, Y. Xie, W. Zhou and W. Yao, *Ultrason. Sonochem.*, 2020, **64**, 104844.
31 F. Penteado, B. Monti, L. Sancineto, G. Perin, R. G. Jacob, C. Santi and E. J. Lenardão, *Asian J. Org. Chem.*, 2018, **7**, 2368–2385.
32 Z. Zhao, Y. Xue, G. Xu, D. Chen, J. Zhou, P. Liu, S. Han and H. Lin, *Int. J. Energy Res.*, 2017, **41**, 1081–1095.
33 M. K. Elmkaddem, P. De Caro, S. Thiébaud-Roux, Z. Mouloungui and E. Vedrenne, *OCL: Oilseeds Fats, Crops Lipids*, 2016, **23**(5), D507.
34 A. Nikseresht, A. Daniyali, M. Ali-Mohammadi, A. Afzalinia and A. Mirzaie, *Ultrason. Sonochem.*, 2017, **37**, 203–207.
35 A. Afzalinia, A. Mirzaie, A. Nikseresht and T. Musabeygi, *Ultrason. Sonochem.*, 2017, **34**, 713–720.
36 H. Veisi, A. Nikseresht, A. Rostami and S. Hemmati, *Res. Chem. Intermed.*, 2019, **45**, 507–520.
37 W. Xue, D. Huang, X. Wen, S. Chen, M. Cheng, R. Deng, B. Li, Y. Yang and X. Liu, *J. Hazard. Mater.*, 2020, **390**, 122128.
38 F. Lorignon, A. Gossard and M. Carboni, *Chem. Eng. J.*, 2020, **393**, 124765.
39 N. Shekarlab, R. Ghorbani-Vaghei and S. Alavinia, *J. Organomet. Chem.*, 2021, **949**, 121971.
40 M. Younas, M. Rezakazemi, M. Daud, M. B. Wazir, S. Ahmad, N. Ullah, Inamuddin and S. Ramakrishna, *Prog. Energy Combust. Sci.*, 2020, **80**, 100849.
41 L. Yang, H. Zhang, P. Tao, X. Lu, X. Li, C. Wang, B. Wang, F. Yue, D. Zhou and Q. Xia, *ACS Appl. Mater. Interfaces*, 2021, **13**, 8474–8487.
42 A. Dhakshinamoorthy, A. M. Asiri and H. Garcia, *ACS Catal.*, 2019, **9**, 1081–1102.
43 M. Koolivand, M. Nikoorazm, A. Ghorbani-Choghamarani, M. Mohammadi, A. Ghorbani-Choghamarani and M. Mohammadi, *Appl. Organomet. Chem.*, 2022, **36**, e6656.
44 S. M. Ramish, A. Ghorbani-Choghamarani and M. Mohammadi, *Sci. Rep.*, 2022, **12**, 1479.
45 N. Hussain-Khil, A. Ghorbani-Choghamarani and M. Mohammadi, *Sci. Rep.*, 2021, **11**, 15657.
46 A. Nikseresht, S. Ghasemi and S. Parak, *Polyhedron*, 2018, **151**, 112–117.
47 J. Babamoradi, R. Ghorbani-Vaghei and S. Alavinia, *Can. J. Chem.*, 2022, **100**, 412–421.
48 R. Oozeerally, D. L. Burnett, T. W. Chamberlain, R. J. Kashtiban, S. Huband, R. I. Walton and V. Degirmenci, *ChemCatChem*, 2021, **13**, 2517–2529.
49 R. Oozeerally, S. D. K. Ramkhelawan, D. L. Burnett, C. H. L. Tempelman and V. Degirmenci, *Catalysts*, 2019, **9**, 812.
50 R. Oozeerally, D. L. Burnett, T. W. Chamberlain, R. I. Walton and V. Degirmenci, *ChemCatChem*, 2018, **10**, 706–709.
51 T. W. Chamberlain, V. Degirmenci and R. I. Walton, *ChemCatChem*, 2022, **14**, e202200135.
52 H. Chen, Y. Liu, T. Cai, W. Dong, L. Tang, X. Xia, L. Wang and T. Li, *ACS Appl. Mater. Interfaces*, 2019, **11**, 28791–28800.
53 H. Chen, W. Zeng, Y. Liu, W. Dong, T. Cai, L. Tang, J. Li and W. Li, *ACS Appl. Mater. Interfaces*, 2021, **13**, 16364–16373.
54 J. Guo, J. Wu, Y. Guan, J. Wang, Q. Liu, X. Mao, X. Qi, P. He and H. Wang, *Energy Fuels*, 2021, **35**, 3252–3265.
55 R. El Osta, A. Carlin-Sinclair, N. Guillou, R. I. Walton, F. Vermoortele, M. Maes, D. de Vos and F. Millange, *Chem. Mater.*, 2012, **24**, 2781–2791.
56 P. L. Llewellyn, P. Horcajada, G. Maurin, T. Devic, N. Rosenbach, S. Bourrelly, C. Serre, D. Vincent, S. Loera-Serna, Y. Filinchuk and G. Férey, *J. Am. Chem. Soc.*, 2009, **131**, 13002–13008.
57 S. Ghasemi, M. Yousefi, A. Nikseresht and H. Omidi, *Process Biochem.*, 2021, **102**, 92–101.
58 Y. Dou, H. Zhang, A. Zhou, F. Yang, L. Shu, Y. She and J.-R. Li, *Ind. Eng. Chem. Res.*, 2018, **57**, 8388–8395.
59 J. Chen, R. Liu, Y. Guo, L. Chen and H. Gao, *ACS Catal.*, 2015, **5**, 722–733.
60 K. Manna, P. Ji, F. X. Greene and W. Lin, *J. Am. Chem. Soc.*, 2016, **138**, 7488–7491.
61 F. Ghobakhloo, D. Azarifar, M. Mohammadi, H. Keypour and H. Zeynali, *Inorg. Chem.*, 2022, **61**, 4825–4841.
62 A. Ghorbani-Choghamarani, R. Sahraei, Z. Taherinia and M. Mohammadi, *J. Iran. Chem. Soc.*, 2021, **18**, 827–838.
63 Y. Zhang, V. Degirmenci, C. Li and E. J. M. Hensen, *ChemSusChem*, 2011, **4**, 59–64.
64 G. Cai, P. Yan, L. Zhang, H.-C. Zhou and H.-L. Jiang, *Chem. Rev.*, 2021, **121**(20), 12278–12326.
65 Z. Zhuang and D. Liu, *Nano-Micro Lett.*, 2020, **12**, 132.
66 A. Valverde-Gonzalez, M. Iglesias and E. M. Maya, *Chem. Mater.*, 2021, **33**(17), 6616–6639.
67 A. Modak, A. Ghosh, A. R. Mankar, A. Pandey, M. Selvaraj, K. K. Pant, B. Chowdhury and A. Bhaumik, *ACS Sustainable Chem. Eng.*, 2021, **9**(37), 12431–12460.
68 H. Zhang, H. Yang, Z. Pan and Q. Cheng, *React. Chem. Eng.*, 2022, **7**, 1626–1639.
69 L. Peng, X. Gao, Y. Liu, J. Zhang and L. He, *Energy Fuels*, 2021, **35**, 4182–4190.
70 M. J. Hülsey, B. Zhang, Z. Ma, H. Asakura, D. A. Do, W. Chen, T. Tanaka, P. Zhang, Z. Wu and N. Yan, *Nat. Commun.*, 2019, **10**, 1330.
71 S. Li, Z. Chen, X. Ling, J. Cao, Q. Wang, Y. Zhou and J. Wang, *Appl. Surf. Sci.*, 2019, **496**, 143650.
72 Y. Shi, Z. Guo, Q. Wang, L. Zhang, J. Li, Y. Zhou and J. Wang, *ChemCatChem*, 2017, **9**, 4426–4436.
73 S. Xiong, Y. Guan, C. Luo, L. Zhu and S. Wang, *Energy Fuels*, 2021, **35**, 14462–14483.
74 R. Al-Faze, E. F. Kozhevnikova and I. V. Kozhevnikov, *ACS Omega*, 2021, **6**, 9310–9318.
75 B. Zhang, H. Asakura, J. Zhang, J. Zhang, S. De and N. Yan, *Angew. Chem.*, 2016, **128**, 8459–8463.
76 J. Gordon, H. Kazemian and S. Rohani, *Microporous Mesoporous Mater.*, 2012, **162**, 36–43.
77 A. Nikseresht and E. Aderang, *Appl. Chem.*, 2021, **16**, 25–38.
78 J. Gordon, H. Kazemian and S. Rohani, *Mater. Sci. Eng., C*, 2015, **47**, 172–179.
79 P. Dinh Du and P. Ngoc Hoai, *Adv. Mater. Sci. Eng.*, 2021, **2021**, 1–13.
80 E. Yılmaz, E. Sert and F. S. Atalay, *J. Taiwan Inst. Chem. Eng.*, 2016, **65**, 323–330.
81 M. Shi, S.-C. Cui and W.-P. Yin, *Eur. J. Org. Chem.*, 2005, **2005**, 2379–2384.

82 A. R. Pourali and A. Goli, *J. Chem. Sci.*, 2011, **123**, 63–67.
83 M. A. Zolfigol, E. Madrakian and E. Ghaemi, *Indian J. Chem., Sect. B: Org. Chem. Incl. Med. Chem.*, 2001, **40**, 1191–1195.
84 W.-B. Pan, L.-M. Wei, L.-L. Wei, C.-C. Wu, F.-R. Chang and Y.-C. Wu, *J. Chin. Chem. Soc.*, 2005, **52**, 581–588.
85 A. Ghorbani-Choghamarani, H. Goudarziafshar, M. Nikoorazm and S. Yousefi, *Can. J. Chem.*, 2009, **87**, 1144–1147.